*Optica Applicata, Vol. XXXIX, No. 3, 2009*

# Fabrication and photoelectrical properties of a novel violet and blue enhanced SINP silicon photovoltaic device

HEBO[1], ZHONGQUANMA[1], XUJING[2], ZHAOLEI[1], ZHANGNANSHENG[1], LIFENG[1], SHENCHENG[1], SHENLING[1], MENGXIAJIE[1], ZHOUCHENGYUE[1], YUZHENGSHAN[1], YINYANTING[1]

[1]SHU-Solar E PV Laboratory, Department of Physics, Shanghai University, Shanghai 200444, China

[2]State Key Laboratory of Advanced Technology for Materials Synthesis and Processing, WuHan University of Technology, HuBei WuHan 430070, China

A novel ITO/$SiO_2$/*np*-silicon violet and blue enhanced photovoltaic device with SINP structure has been fabricated by thermal diffusion of phosphorus. The shallow junction was formed to enhance the spectral responsivity within the wavelength range of 400–600 nm. An ultrathin silicon dioxide was thermally grown at low temperature and RF sputtering of ITO antireflection coating to reduce the reflected light and enhance the sensitivity. The crystalline structure, optical and electric properties of ITO film were determined by an XRD, UV-VIS spectrophotometer, a four point probe and the Hall effect measurement, respectively. The results show that ITO film has high quality. The current-voltage (*I-V*) characteristics, spectral response and responsivity of the photovoltaic device with high quantum efficiency of violet SINP and deep junction SINP structure were calculated and analyzed in detail.

Keywords: ITO, SINP photovoltaic device, current-voltage (*I-V*) characteristics, spectral response, responsivity.

## 1. Introduction

Violet and blue enhanced semiconductor photovoltaic devices are required for various applications such as optoelectronic devices for communication, solar cell, aerospace, spectroscopic and radiometric measurements [1]. The development of semiconductor *p-n* junction photodetector is based both on the principle of internal photoelectric effect and on the theory of *p-n* junction. These applications require low dark current and high short-wavelength responsivity and stability [2]. Silicon photodetectors are sensitive from infrared to visible light but have poor responsivity in the short wavelength region. Because the light is absorbed exponentially with distance and is proportional to the absorption coefficient of crystal silicon, the absorption coefficient is very high for shorter wavelengths in the violet region and is small for longer wavelengths. Hence, short wavelength photons such as violet and blue are absorbed in a thin top surface

layer, for 90% absorption of the incident radiation at $\lambda = 360$ nm the absorption depth is 115 nm,while silicon becomes transparent to light wavelengths longer than 1200 nm. If the surface recombination of the photogenerated electron-hole (e-h) pairs is high, then these e-h pairs will undergo recombination before being collected. Furthermore, the heavily doped emitter may contain a dead layer near the surface resulting in poor quantum efficiency of the photoelectric device under short wavelength region [3].

In the paper, in order to improve the responsivity of silicon photodetector at 400–600 nm, a novel ITO/$SiO_2$/*np* Si SINP violet and blue enhanced photovoltaic device (SINP is the abbreviation of semiconductor/insulator/*np* structure) was successfully fabricated using thermal diffusion of phosphorus for shallow junction, an ultrathin silicon dioxide and ITO film as an antireflection/passivation layer. Figures 1 and 2 show the schematic and bandgap structure of the novel SINP photovoltaic device. The ultrathin $SiO_2$ film not only effectively passivates the surface of Si, but also reduces the mismatch between ITO and Si, since a low surface recombination is imperative for good quantum efficiency of the device at short wavelength. The ITO film is highly conducting, antireflective (especially for violet and blue light) and stable. In addition, a wide gap semiconductor as the top film can serve as a low-resistance window, as well as the collector layer of the junction. Therefore, it can eliminate the disadvantage of high sheet resistance, which results from shallow junction. Because the penetration depth of short wavelength light is thin, the shallow junction is in favor of improving sensitivity. In this paper, violet and near-infrared SINP photovoltaic devices with two types of junction depth have been made.

## 2. Experimental procedure

The SINP photovoltaic device was manufactured using state-of-the-art technology including clean-room facilities, thermal diffusion of phosphorus, low temperature thermally grown oxidation, RF sputtering ITO antireflection film, a shadow metal mask, metal vacuum evaporating and sputtering, *etc*.

The starting material was *p*-type CZ silicon with a boron-doping concentration corresponding to 2 Ωcm. The thickness of the wafers used was 220 μm and the crystal orientation was (100). After RCA cleaning process and chemical preparation for having the distorted layer removed and texturized, the shallow and deep junction emitters for blue and near-infrared enhanced SINP photovoltaic devices were generated at temperatures of 850 °C for 20 min and 920 °C for 30 min, in an open quartz tube using liquid $POCl_3$ as the doping source. The result is emitters with sheet resistance 37 Ω/□ and 10 Ω/□. The junction depth of shallow and deep junction is 0.35 μm and 1 μm.

After phosphorus-silicon glass removal, a 2 μm Al metal electrode was deposited on the *p*-silicon as the bottom electrode by vacuum evaporation. A 15–20 Å thin silicon oxide film was successfully thermally grown at low temperature (500 °C for 20 min in $N_2$:$O_2$ = 4:1 condition).

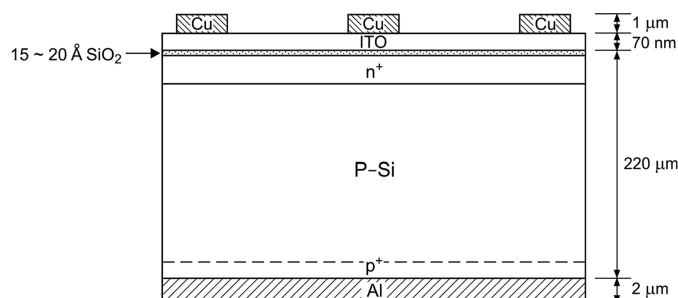


Fig. 1. Schematic of the novel SINP photovoltaic device.

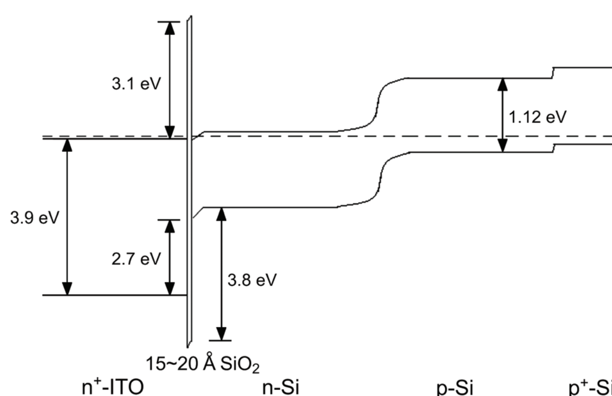


Fig. 2. Bandgap structure of the novel SINP photovoltaic device.

A 70 nm ITO antireflection film was deposited on the substrate in a RF magnetron sputtering system. The target was a sintered ceramic disk of $In_2O_3$ doped with 10 wt% $SnO_2$ (purity 99.99%). The base pressure inside the chamber was pumped down to less than $3\times10^{-4}$ Pa. The sputtering was carried out at a working gas (pure Ar) pressure of 1 Pa. The Ar flow ratio was 30 sccm. The RF power and the substrates were 100 W and 300 °C. The sputtering was processed for 0.5 h. The ITO films were also prepared on glass to investigate the optical and electrical properties.

Finally, by sputtering, a 1 μm Cu metal film was deposited with a shadow mask on the ITO surface for the top grids electrode. The area of the device was 4 $cm^2$.

The thickness of ITO film was measured by stylus profiler. Crystalline structure of the films was investigated by XRD. The optical transmission of the films was measured by UV-VIS spectrophotometer. The electrical properties of ITO films were determined by a four point probe and the Hall effect measurement (Accent HL5500pc). The current-voltage ($I$-$V$) characteristics of the device were measured by Agilent 4155C semiconductor parameter analyzer. The spectral response and responsivity of the devices were obtained for the wavelength range between 400 nm and 1100 nm by the spectral response measurement for photoelectric cell.

## 3. Results and discussion

### 3.1. Crystalline structure, optical and electric properties of ITO films

Figure 3 shows the XRD spectrum of ITO film on glass, which was deposited by RF magnetron sputtering. The dominant peak located at 30.23° is attributed to the ITO (222) diffraction. The results indicate that the film has a bixbyite structure with its dominant orientation along the (222) perpendicular to the substrate surface.

In order to obtain more structural information and evaluate the mean grain size $D$ of the films, we adopted the Scherrer formula:

$$D = \frac{0.9\lambda}{\beta \cos\theta} \tag{1}$$

where $\lambda$, $\theta$ and $\beta$ are the X-ray wavelength (1.54056 Å), the Bragg diffraction angle, and the FWHM of ITO (222) diffraction peak, respectively. The mean grain size of the film was 7.2 nm.

In order to learn the optical absorption and energy band structure of ITO film, the transmission spectrum of the ITO film deposited on the glass substrate has been

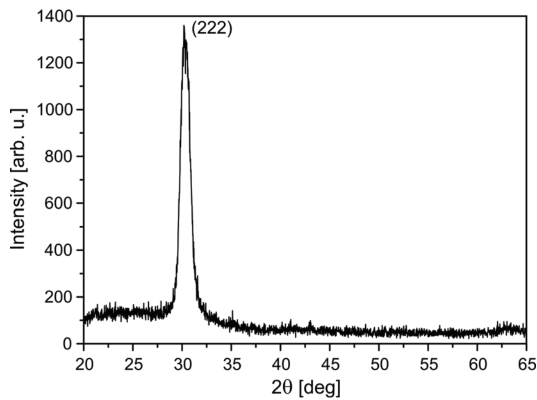


Fig. 3. XRD spectrum of the ITO film on glass.

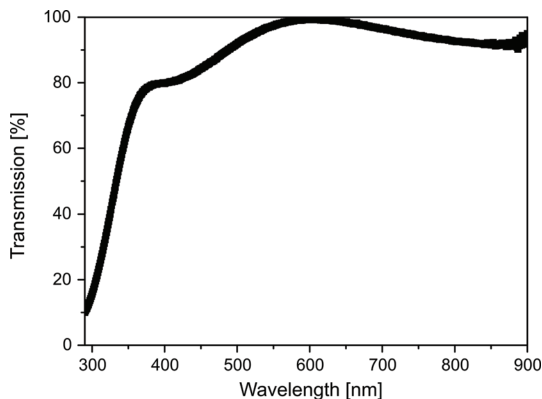


Fig. 4. Transmission spectrum of the ITO film.

measured, as shown in Fig. 4. The thickness of ITO film is about 700 Å. The average transmittance of the film is about 95% in the visible region. The absorption coefficient $\alpha$ was evaluated from the measurements of optical transmittance $T$ according to the following relation [4]:

$$\alpha = \frac{1}{d} \ln \frac{1}{T} \tag{2}$$

where $d$ is the thickness of ITO film. The optical band gap of ITO film is determined through the extrapolation of linear part of the absorption edge to $\alpha = 0$ in the relationship as:

$$(\alpha h\nu)^2 = A(E_g - h\nu) \tag{3}$$

This result is basically from the intrinsic absorption of electronic transition and the value of about 3.9 eV (see Fig. 5).

Figure 6 indicates the reflection loss for ITO film on a texturized surface Si from UV to the violet, and blue regime is much lower than that of $Si_3N_4$ film, which are

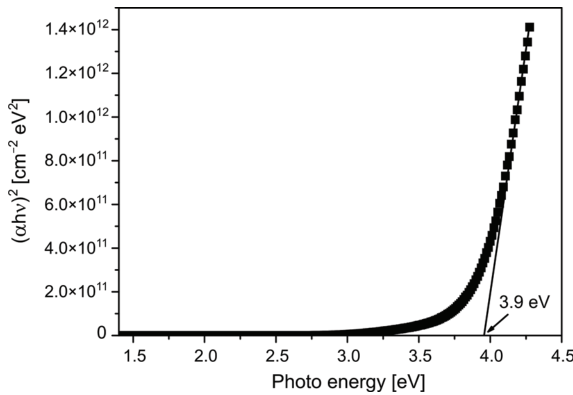


Fig. 5. Variation of $(ah\nu)^2$ vs. $h\nu$ of ITO film.

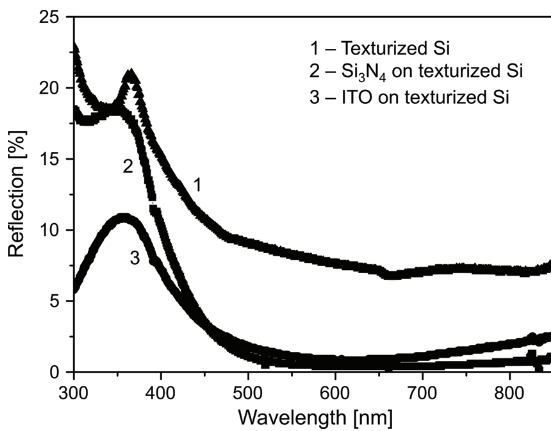


Fig. 6. The comparison of reflection loss for ITO on texturized Si, $Si_3N_4$ on texturized Si and bare texturized Si surface.

widely made by plasma enhanced chemical vapour deposition (PECVD) technology. In the visible regime, reflection loss for ITO film is as low as in the case of $Si_3N_4$ film. This shows that ITO optical film effectively reduces reflection loss in short- -wavelength, which is suitable for antireflection coating in violet and blue photovoltaic devices.

Electrical properties of the ITO film were determined by a four-point probe and the Hall effect measurement. The square resistance and the resistivity are as low as 17 Ω/□ and $1.19\times10^{-4}$ Ωcm, and the carrier concentration is as high as $2.11\times10^{21}$ atom/cm$^3$.

### 3.2. *I-V* characteristics

Figure 7 shows the current-voltage characteristic of the violet SINP device measured at room temperature in the dark. The *I-V* curves of devices show fairly good rectifying behaviors. Based on the dark current as a function of the applied bias, the corresponding diode resistance defined as $R_D = (dI/dV)^{-1}$ [5] is derived and shown in Fig. 8. The series resistance arising from ohmic depletion plays a dominant role when the forward bias is larger than 0.25 V. When the voltage is between 0.2 V and −0.2 V, the resistance slightly increases as the diffusion current in the base region. When the inversion voltage increases from −0.2 to −0.5 V, the leakage current and the recombination

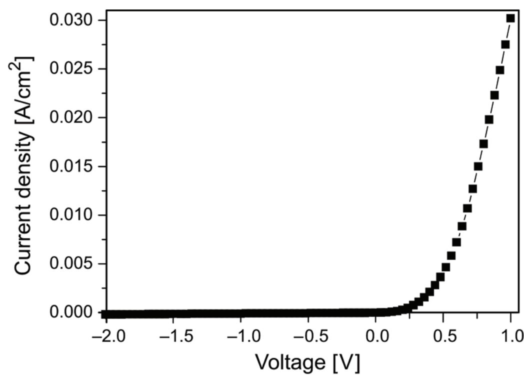


Fig. 7. *I-V* curve of the violet and blue enhanced (shallow junction) SINP photovoltaic device in the dark.

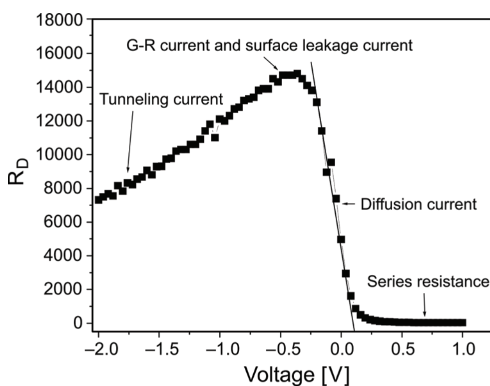


Fig. 8. The variation of SINP violet and blue enhanced SINP device resistance via voltage ($R_D$-$V$ curve).

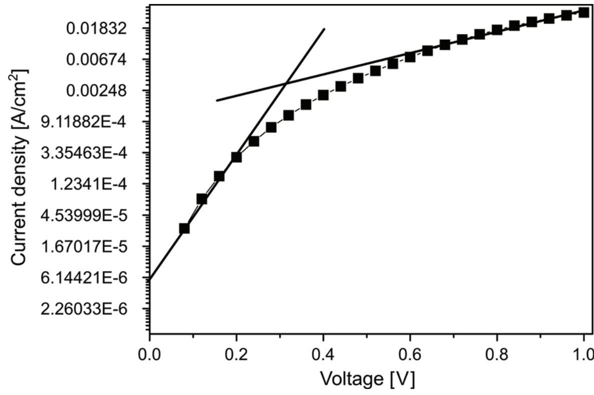


Fig. 9. The corresponding logarithmic scale in current with forward bias condition for violet and blue enhanced SINP device.

current in the surface layers restrain the increase of the dynamic resistance, which keeps the $R_D$-$V$ curve in an invariable state. In the high inversion voltage region, the tunneling current plays a dominant role.

The plot of $\ln(J)$ against $V$, is shown in Fig. 9, which indicates that the current at low voltage($V < 0.3$ V) varies exponentially with voltage. The characteristics can be described by the stand diode equation: $J = J_0[\exp(qV/nk_BT) - 1]$ where $q$ is the electronic charge, $V$ is the applied voltage, $k_B$ is the Boltzmann constant, $n$ is the ideality factor, and $J_0$ is the saturation current density [6, 7]. Calculation of $J_0$ and $n$ from measurements in Fig. 9. The value of the ideality factor of the violet SINP device is determined from the slop of the straight line region of the forward bias log *I*-*V* characteristics. At low forward bias ($V < 0.2$ V), the typical values of the ideality factors and the reverse saturation current density are 1.84 and $5.58\times10^{-6}$ A/cm$^2$, respectively. Using the standard diode equation $J = J_0[\exp(qV/nk_BT) - 1]$, where $n = 1.84$ and $J_0 = 5.58\times10^{-6}$ A/cm$^2$. The result of calculation (using standard diode equation) is similar to the measured *I*-*V* curve. By the same calculation method, the ideality factor and the reverse saturation current density of deep junction SINP photovoltaic device are 2.21 and $4.2\times10^{-6}$ A/cm$^2$. This result indicates that the recombination current ($J_r \approx \exp(qV/2kT)$) dominates in the forward current. The rectifying behaviors and compositions of dark current for violet SINP photovoltaic device are better than those of the deep junction SINP device, because the ideality factor of violet SINP photovoltaic device ($n = 1.84$) is lower than the ideality factor of deep junction SINP device ($n = 2.21$). And the values of $I_F/I_R$ ($I_F$ and $I_R$ stand for forward and reverse current, respectively) at 1 V for violet SINP device and deep junction SINP device are found to be as high as 324.7 and 98.4, respectively.

The photo *I*-*V* characteristics were measured by illuminating the novel SINP devices with low power white light (6.3 mW/cm$^2$). It is observed that both of the novel SINP devices exhibit great photovoltaic effect and rectifying behavior in the presence of light, too. Figures 10 and 11 show that the photocurrent (short-

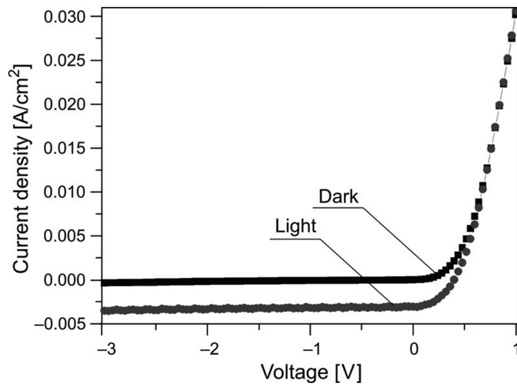


Fig. 10. *I-V* characteristic of the violet and blue enhanced SINP photovoltaic device in the dark and in light (6.3 $mW/cm^2$ white light).

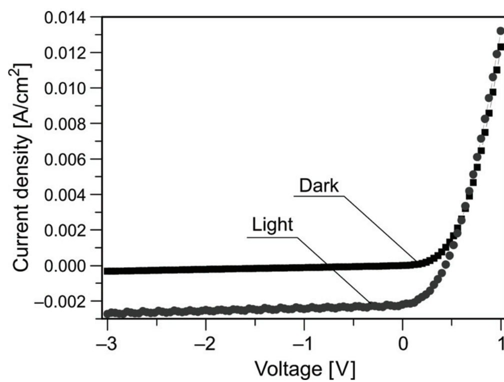


Fig. 11. *I-V* characteristic of the deep junction SINP device in the dark and in light (6.3 $mW/cm^2$ white light).

-circuit current) density of violet and blue enhanced SINP photovoltaic device ($3.08\times10^{-3}$ $A/cm^2$) is much higher than the photocurrent density of deep junction SINP device ($2.23\times10^{-3}$ $A/cm^2$).

### 3.3. Spectral response and responsivity

The spectral response and responsivity of the devices were measured between the wavelengths of 400 nm and 1100 nm. In the visible light region, the internal quantum efficiencies (IQE) for both devices are high over a range from 77% to 83%, see Fig. 12. The IQE of device was determined from the following relation: $IQE\cdot(1-R)=EQE$, where $R$ is the reflectance loss [8]. The ITO antireflection coating effectively reduced reflection loss in short-wavelength to visible light. Therefore, the external quantum efficiencies (EQE) for both devices are also high over a range from 70% to 78%, see Fig. 13.

Figures 12 through 14 show the comparison of IQE, EQE and responsivity for violet and blue SINP photovoltaic device and deep junction SINP photovoltaic device. In the violet and blue region, the IQE and EQE of shallow junction violet SINP device

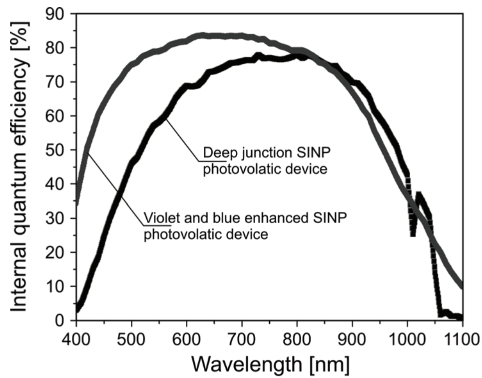


Fig. 12. The comparison of internal quantum efficiency for violet and blue SINP photovoltaic device and deep junction SINP photovoltaic device.

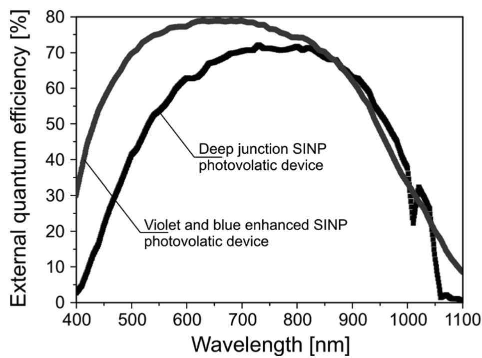


Fig. 13. The comparison of external quantum efficiency for violet and blue enhanced SINP photovoltaic and deep junction SINP photovoltaic device.

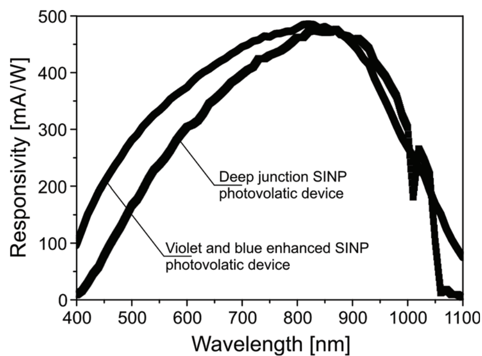


Fig. 14. The comparison of responsivity for violet and blue SINP photovoltaic device and deep junction SINP photovoltaic device.

are much higher than those of the deep junction SINP device. For example, the EQE and responsivity of the violet SINP device are 70% and 285 mA/W at 500 nm, while the EQE and responsivity of the deep junction SINP device are 42% and 167 mA/W at 500 nm, respectively. The peak of violet and blue SINP photovoltaic device spectral responsivity is 487 mA/W at about 800 nm, while the peak of deep junction SINP photovoltaic device spectral responsivity is 471 mA/W at about 860 nm.

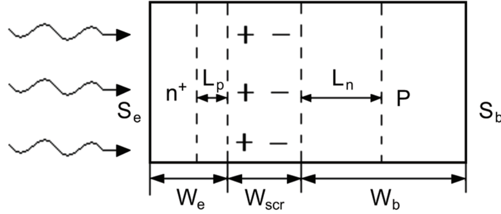


Fig. 15. The structure of $n^+p$ junction for photovoltaic device.

The structure of $n^+p$ junction of photovoltaic device is shown in Fig. 15. $\Delta p(x)$ generated in the *n*-emitter of the device can be obtained by solving the steady-state continuity equation given by [9]

$$D_p \frac{d^2 \Delta p(x)}{dx^2} - \frac{\Delta p(x)}{\tau_p} + \alpha \phi_0 (1 - R) e^{-\alpha x} = 0 \tag{4}$$

while $\Delta n(x)$ generated in the *p*-base of the device can also be obtained by solving the steady-state continuity equation

$$D_n \frac{d^2 \Delta n(x)}{dx^2} - \frac{\Delta n(x)}{\tau_n} + \alpha \phi_0 (1 - R) e^{-\alpha x} = 0 \tag{5}$$

the hole current density at $x = W_e$

$$J_p = -qD_p \left.\frac{d\Delta p}{dx}\right|_{x = W_e} \tag{6}$$

the electron photocurrent density at the depletion edge of the *p*-base region

$$J_n = qD_n \left.\frac{d\Delta n}{dx}\right|_{x = W_e + W_{\mathrm{scr}}} \tag{7}$$

the photocurrent density generated in the depletion region

$$J_d = q \int_{W_e}^{W_e + W_{\mathrm{scr}}} g_E \, dx = q \phi_0 (1 - R) e^{-\alpha W_e} \left[ 1 - e^{-\alpha W_{\mathrm{scr}}} \right] \tag{8}$$

the total photocurrent density is equal to the sum of photocurrent density generated in *n*-emitter, *p*-base and space-charge regions.

$$J_L = J_{\mathrm{total}}(\lambda) = J_p(\lambda) + J_n(\lambda) + J_d(\lambda) = J_e(\lambda) + J_b(\lambda) + J_{\mathrm{scr}}(\lambda) \tag{9}$$

the internal quantum efficiency for a *p-n* junction photovoltaic device can be expressed by

$$\eta = \frac{J_L(\lambda)}{q\phi_0(1-R)} \times 100\% = \eta_e + \eta_b + \eta_{\text{scr}} \tag{10}$$

Therefore, by Tab. 1, the internal quantum efficiency for $n^+$-emitter can be expressed by

$$\eta_e = \frac{\alpha L_e}{(\alpha L_e)^2 - 1}\left[\frac{S_e + \alpha L_e - \left(S_e \cosh\frac{W_e}{L_e} + \sinh\frac{W_e}{L_e}\right)e^{-\alpha W_e}}{S_e \sinh\frac{W_e}{L_e} + \cosh\frac{W_e}{L_e}} - \alpha L_e e^{-\alpha W_e}\right] =$$

$$= \frac{0.1\alpha}{(0.1\alpha)^2 - 1}\left[\frac{20 + 0.1\alpha - 573.3e^{-0.4\alpha}}{573.3} - 0.1\alpha e^{-0.4\alpha}\right] \tag{11}$$

where $S_e = s_e L_e / D_e = 20$. The internal quantum efficiency for space-charge region can be expressed by

$$\eta_{\text{scr}} = e^{-\alpha W_e}\left(1 - e^{-\alpha W_{\text{scr}}}\right) = e^{-0.4\alpha}\left(1 - e^{-0.5\alpha}\right) \tag{12}$$

The internal quantum efficiency for *p*-base can be expressed by

$$\eta_b = \frac{\alpha L_b}{(\alpha L_b)^2 - 1} e^{-\alpha(W_e + W_{\text{scr}})}\left[\alpha L_b - \frac{S_b \cosh\frac{W_b}{L_b} + \sinh\frac{W_b}{L_b} + (\alpha L_b - S_b)e^{-\alpha W_b}}{S_b \sinh\frac{W_b}{L_b} + \cosh\frac{W_b}{L_b}}\right]$$

$$= \frac{50\alpha}{(50\alpha)^2 - 1} e^{-0.9\alpha}\left[50\alpha - \frac{67897 + (50\alpha - 1666)e^{-220\alpha}}{67880}\right] \tag{13}$$

where $S_b = s_b L_b / D_b = 1666$. The total internal quantum efficiency for a *p-n* junction photovoltaic device can be expressed by

$$\eta_{\text{total}} = \eta_e + \eta_{\text{scr}} + \eta_b \tag{14}$$

In the above equations, $\alpha$ is the absorption coefficient of the crystal silicon material, it is a function of wavelengths. Using the absorption coefficient for various

T a b l e 1. The violet SINP photovoltaic device parameters for the simulation.

| Region | Width | Diffusion coefficient | Minority carrier lifetime | Diffusion length | Surface recombination rate |
|---|---|---|---|---|---|
| $n^+$-emitter | $W_e = 0.4$ μm (junction depth) | $D_e = 5$ cm$^2$/S | $\tau_e = 2\times10^{-11}$ s | $L_e = 0.1$ μm | $S_e = 1\times10^7$ cm/s |
| Space-charge | $W_{scr} = 0.5$ μm | | | | |
| $p$-base | $W_b = 220$ μm | $D_b = 30$ cm$^2$/S | $\tau_b = 8\times10^{-7}$s | $L_b = 50$ μm | $S_b = 1\times10^7$ cm/s |

T a b l e 2. The deep junction SINP photovoltaic device parameters for the simulation.

| Region | Width | Diffusion coefficient | Minority carrier lifetime | Diffusion length | Surface recombination rate |
|---|---|---|---|---|---|
| $n^+$-emitter | $W_e = 1$ μm (junction depth) | $D_e = 5$ cm$^2$/S | $\tau_e = 2\times10^{-11}$ s | $L_e = 0.1$ μm | $S_e = 1\times10^7$ cm/s |
| Space-charge | $W_{scr} = 0.5$ μm | | | | |
| $p$-base | $W_b = 220$ μm | $D_b = 30$ cm$^2$/S | $\tau_b = 8\times10^{-7}$ s | $L_b = 50$ μm | $S_b = 1\times10^7$ cm/s |

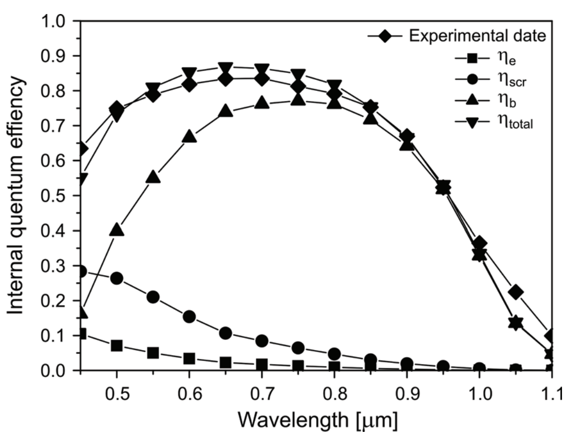


Fig. 16. Measured IQE of a violet SINP device and the calculated spectral response.

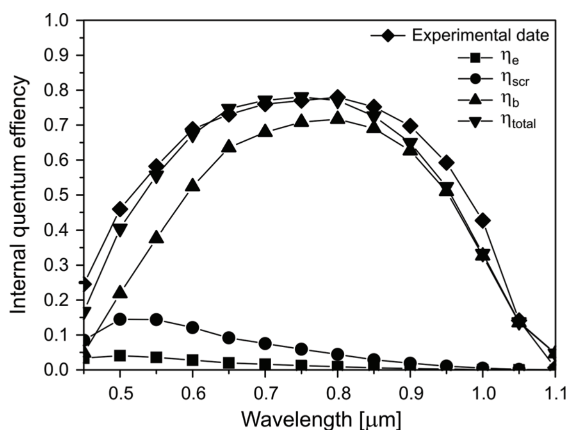


Fig. 17. Measured IQE of a deep junction SINP device and the calculated spectral response.

wavelengths in formulae (11)–(14), Fig. 16 shows that the calculated results are consistent with the experimental data. By the same calculation method and Tab. 2, Fig. 17 shows the calculated spectral response and measured IQE of a deep junction SINP device.

The calculated results indicate that the high quantum efficiency and responsivity of violet and blue enhanced photovoltaic cell is attributed to the shallow junction and the well conducting, violet and blue antireflection coating of ITO optical film.

## 4. Conclusions

The novel ITO/$SiO_2$/*np* silicon SINP violet and blue enhanced photovoltaic device has been fabricated by thermal diffusion of phosphorus for shallow junction to enhance the spectral responsivity within the wavelength range of 400–600 nm. An ultrathin silicon dioxide thermally grown at low temperature and RF sputtering of ITO antireflection coating to reduce the reflected light and enhance the sensitivity. The ITO film was performed to be of high quality by XRD, UV-VIS spectrophotometer, a four point probe and the Hall effect measurement. Fairly good rectifying and great photovoltaic behaviors are tested and analyzed by *I-V* measurements. The spectral response and responsivity of high quantum efficiency of violet SINP photovoltaic device and deep junction SINP photovoltaic device were calculated and analyzed in detail. The results indicate that the novel violet and blue enhanced photovoltaic device can be used not only for high quantum efficiency of violet and blue enhanced silicon photodetector for various applications, but also used for high efficiency solar cell.

*Acknowledgments* – This work was partly supported by the Natural Science Foundation of China (No. 60876045), Shanghai Leading Academic Discipline Project (S30105), Innovation Foundation of Shanghai Education Committee (No. 08YZ12), R&D Foundation of SHU-SOENs PV Joint Lab. (SS-E0700601).

### References

[1] CANFIELD L.R., KERNER J., KORDE R., *Silicon photodiodes optimized for the EUV and soft x-ray regions*, Proceedings of SPIE **1344**, 1990, pp. 372–377.

[2] LIUENKE, *et al*., *Semiconductor Physics*, Electronic Industry Publishing House, Beijing 2003 (in Chinese).

[3] XIANSONG FU, SUYING YAO, JIANGTAO XU, YAO LU, YUNGUANG ZHENG, *Study on high signal-to-noise ratio (SNR) silicon p-n junction photodetector*, Optica Applicata **36**(2–3), 2006, pp. 421–428.

[4] SELMI M., CHAABOUNI F., ABAAB M., REZIG B., *Studies on the properties of sputter-deposited Al-doped ZnO films*, Superlattices and Microstructures **44**(3), 2008, pp. 268–275.

[5] CHEN X.D., LING C.C., FUNG S., BELING C.D., MEI Y.F., FU R.K.Y., SIU G.G., CHU P.K., *Current transport studies of ZnO/p-Si heterostructures grown by plasma immersion ion implantation and deposition*, Applied Physics Letters **88**(13), 2006, p. 132104.

[6] MRIDHA S., DUTTA M., BASAK D., *Photoresponse of n-ZnO/p-Si heterojunction towards ultraviolet/ visible lights: thickness dependent behavior*, Journal of Materials Science: Materials in Electronics **20**(Supplement 1), 2009, pp. 376–379.

[7] MRIDHA S., BASAK D., *Ultraviolet and visible photoresponse properties of n-ZnO/p-Si heterojunction*, Journal of Applied Physics **101**(8), 2007, p. 083102.
[8] KITTIDACHACHAN P., MARKVART T., BAGNALL D.M., GREEF R., ENSELL G.J., *A detailed study of p-n junction solar cells by means of collection efficiency*, Conference Record of the 2006 IEEE 4th World Conference on Photovoltaic Energy Conversion, Vol. 1, 2006, pp. 1130–1133.
[9] SZE S.M., *Physics of Semiconductor Devices*, Xian Jiaotong University Press, Xian 2007 (in Chinese).

*Received February 16, 2009*
*in revised form March 23, 2009*